Self and Mutual Inductance Behavioral Modeling of Square-Shaped IPT Coils With Air Gap and Ferrite Core Plates

ALBERTO DELGADO[1], (Student Member, IEEE), **GIULIA DI CAPUA**[2], (Senior Member, IEEE),
KATERYNA STOYKA[3], **LIXIN SHI**[1], (Student Member, IEEE),
NICOLA FEMIA[3], (Senior Member, IEEE), **ANTONIO MAFFUCCI**[2], (Senior Member, IEEE),
SALVATORE VENTRE[2], (Senior Member, IEEE), **PEDRO ALOU**[1], (Member, IEEE),
JESÚS ÁNGEL OLIVER[1], (Member, IEEE), **AND JOSÉ ANTONIO COBOS**[1], (Fellow, IEEE)

[1]Centro de Electrónica Industrial, Universidad Politécnica de Madrid, 28006 Madrid, Spain
[2]Department of Electrical and Information Engineering, University of Cassino and Southern Lazio, 03043 Cassino, Frosinone, Italy
[3]Department of Information and Electrical Engineering and Applied Mathematics, University of Salerno, 84084 Fisciano, Salerno, Italy

Corresponding author: Giulia Di Capua (giulia.dicapua@unicas.it)

ABSTRACT The design and optimization of coils for Inductive Power Transfer (IPT) systems is an iterative process conducted in Finite Element (FE) tools that takes a lot of time and computational resources. In order to overcome such limitations in the design process, new empirical equations for the evaluation of the self-inductance and mutual inductance values are proposed in this work. By means of a multi-objective genetic programming algorithm, the self-inductance, the mutual inductance and the coupling factor values obtained from FE simulations of IPT link are accounted by analytical equations, based on the geometric parameters defining the IPT link. The behavioral modeling results are compared with both FE-based and experimental results, showing a good accuracy.

INDEX TERMS Behavioral modeling, finite element analysis, finite element modeling, inductive power transfer, magnetic components, optimization process, wireless power transfer.

I. INTRODUCTION

The design of an Inductive Power Transfer (IPT) link involves system-level specifications that must be matched with a proper choice of architectures and components [1]. System-level requirements usually involve power, voltage and current ratings, switching frequency and source type [2]. In addition, the chosen architecture has an impact in the resonance method [3], [4]. All these requirements must be taken into account in optimizing the system's components, such as the magnetic link (coupled coils). The IPT coil design, however, is subjected to additional constraints, and can be considered as one of the most critical aspects of an IPT system, as it contributes to several performance benchmarks such as minimum efficiency requirement (also under misalignment conditions), safety issue related to leakage magnetic field mitigation, cost, volume and weight [5].

The associate editor coordinating the review of this manuscript and approving it for publication was Diego Oliva.
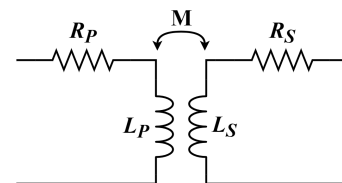

FIGURE 1. Quasi-static equivalent circuit model of the inductive link of an IPT system.

In the quasi-static approximation, the magnetic link can be modeled as a coupled inductor with losses, represented as the two-port element depicted in Fig. 1, where L_P and L_S are the self-inductances at the primary (transmitting side) and the secondary (receiving side), M is the coil mutual inductance, R_P and R_S are the respective coil resistances, and k is the coupling factor, defined as:

$$k = \frac{M}{\sqrt{L_P L_S}} \quad (1)$$

The key-performance indicators at system level are strictly related to these parameters. For instance, once the resonant

method has been chosen, the losses optimization identifies the required values of inductance and coupling factor. Similarly, *L* and *k* have a direct impact on capacitances, switching frequency, and other quantities like the current gain. An optimal design of the IPT link should therefore consider the targeted values of *L* and *k,* as well as the additional physical and geometrical constraints (e.g., weight, maximum footprint allowed, *etc*.). The optimization must be carried out with reference to several design variables (degrees of freedom) that are available when designing a real IPT link, such as: coil shapes, vertical distance (air gap), type of wires, number of turns, shapes and physical characteristics of the magnetic core (ferrites) and conducting shield, and so on. Therefore, if the design can rely on analytical expressions of *L* and *k* as functions of the above design variables, then a one-step optimization procedure may be set up. Indeed, by inverting the above relations, a reverse-engineering procedure can be implemented to synthesize into one step the optimal coil design for the target performance.

Unfortunately, analytical expressions for the inductances are available only for very simple cases, which are far from real-world applications, as it is the case of regularly-shaped coils in air with neither core nor shielding [6]. In all practical applications, the inductances and resistances are extracted from full-numerical 3D models of the magneto-quasi static problem, typically based on Finite Element Method (FEM) or Boundary Element Method (BEM). The numerical model of the IPT link is therefore the tool commonly used to investigate the impact of each design variable on the key parameters [7]. For instance, a FEM model has been used in [8] to optimize the ferrite arrangements and determine the coil turn number for multi-turn spiral coils, whereas in [9] and [10] FEM simulations have been carried out to check the influence of the misalignment of the coils on their nominal position.

A design approach fully based on numerical models has some drawbacks. First of all, the computational cost may become unaffordable, although the cost of the single FEM simulation can be reduced to few minutes by using suitable simplifications (as for instance the equivalent layer for the litz-wire [10]). Indeed, in a one-step design the number of configurations to be simulated becomes huge, since the optimization must be performed over a set of possible design variables, each of which assumes several values in a certain given range. A second drawback is the lack of any qualitative information on the solution that makes hard to understand and foresee the dependence of the output (*L* and *k*) on the single design choice. A final drawback is the applicability of the results, which are strictly valid only for the given IPT system. For the above reasons, the design of the coils of an IPT link is purely iterative, and from an initial reasonable ''guess'' geometry, it is possible to vary all the geometric aspects to obtain the desired features.

An alternative design methodology is investigated in this paper. Our goal is to analytically relate the coil inductances to the design variables of real IPT links, by means of
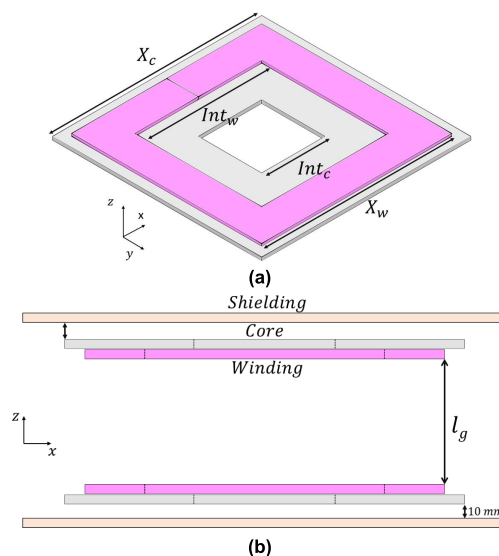
FIGURE 2. (a) A single square-shaped coil and (b) a pair coil with shielding plates.

the so-called ''behavioral models''. These models are identified once for all by using a multi-objective Genetic Programming Algorithm (GPA) and a limited set of FEM-based numerical solutions. This approach provides a solution to all the above issues, by lowering the computational cost, adding qualitative information to the design solutions, and providing a modeling tool that can be easily generalized to a given class of IPT coils.

The class of magnetic links analyzed in this paper is presented in Section II, where major details on the investigated problem are given. Section III is devoted to the derivation of the behavioral models for the inductances of the given class of IPT coils, and to their validation against numerical solutions. These models are successfully validated against experimental measurements, as shown in Section IV. Conclusions are drawn in Section V.

II. PROBLEM STATEMENT

The objective of this paper is to derive analytical relations between the self and mutual inductances of IPT coupled coils and their geometrical parameters. The magnetic link of an IPT systems is a complicated 3D structure, also known as ''pad'', consisting of a pair of coupled coils, a magnetic core made of ferrites, and a conducting shielding.

In this paper, the proposed methodology will be applied to a quite general class of pads, reported in Fig. 2(a), made of two identical square-shaped coils with copper windings (magenta) and ferrite core plates (grey). Fig. 2(b) shows the two identical coils put at a given vertical distance (air gap), with the shielding herein assumed at a distance of 10 mm from each coil. This gap value between the ferrite layer and the aluminum shielding is in line with the typical mechanical dimensions adopted in design standards [12].

We eventually realized a 0.2 millimeter distance between conductors and ferrite plates, resulting in an almost negligible gap between ferrite and winding layers, and a consequent minor effect on self-inductance and mutual inductance values. It is worth highlighting that the behavioral models presented in this paper are valid for square-shaped coils, like those ones shown in Fig. 2. Nevertheless, the findings of the proposed behavioral modeling procedure are general and can be applied to discover new behavioral models for pads with different core geometries and windings distribution, given the relevant FEM-based numerical data.

Given the geometry, the optimal design of this coil pair can be achieved by working on the following 5 quantities (*design variables*):

- Int_C, the lateral dimension of the inner hole in the core plate;
- X_C, the external lateral dimension of the core plate;
- Int_W, the internal lateral dimension of the winding;
- X_W, the external lateral dimension of the winding;
- l_g, the coil pair air gap.

Thus, the ultimate goal of this paper is to derive the analytical expressions that relate the self-inductance L and the mutual inductance M to the design variables $Int_C, X_C, Int_W, X_W, l_g$.

As detailed in the next Section, the procedure to identify such analytical expressions requires as input the values assumed by L and M in a given set of configurations of the above design variables (the "training" set). The validation will then require an additional set of data (the "validation" set). These sets of data are here provided by the numerical solution of the electromagnetic equations in the Magneto-Quasi-Static (MQS) limit, by using a full 3D numerical model. Such a model has been implemented by means of the commercial code Ansys Maxwell [13], based on a differential formulation. An adaptive meshing has been adopted for simulations, and a mesh assessment has been carried out, leading to the mesh of 41613 elements, with which it has been possible to achieve discretization errors lower than 3%. The only simplification introduced with respect to the real pad is the assumption that the coil windings can be modeled as equivalent copper layers, where a uniform current density flows. Indeed, in real pads the coils are made of the so-called Litz wires, which are suitably designed based on the operating frequency, to avoid the skin effect and to reduce the proximity effect in the winding caused by the external magnetic field. This assumption has no effect on the evaluation of the self and mutual inductance, since it only affects the AC resistance, but provides a great benefit in lowering the computational cost of the numerical simulation.

As first preliminary step, the test conditions to be simulated by the 3D-FEM numerical solver have been selected. Given the geometry highlighted in Fig. 2, each coil pair set-up has to fulfil the following dimensional constraints: $Int_C \leq Int_W \leq X_W \leq X_C$. Accordingly, we define the ranges of possible geometrical dimensions for each parameter, as listed in Table 1. Such values are typical for electric vehicle IPT

TABLE 1. Reference dataset of coil geometrical dimensions.

Parameter	Initial value	Final value	Step size	# of values
Int_C	85 mm	235 mm	50 mm	4
Int_W	90 mm	365 mm	25 mm	12
X_W	120 mm	445 mm	25 mm	14
X_C	125 mm	500 mm	25 mm	16
l_g	10 mm	50 mm	20 mm	3

coils. For each value of l_g, we have 2125 possible conditions ensuring that $Int_C \leq Int_W \leq X_W \leq X_C$. However, the number of conditions for each Int_C is not fixed: the greater this value is, the greater the values of Int_W, X_W and X_C are, thus reducing the number of possible conditions for each Int_C. To limit our analysis to only feasible coil designs, geometrical conditions satisfying "practical" constraints on the coil dimensions have been introduced. These conditions are summarized by constraints (2):

$$Int_C \geq 0.6 Int_W \quad (2.a)$$

$$X_C \leq 1.4 X_W \quad (2.b)$$

$$X_W \geq 1.2 Int_W \quad (2.c)$$

The constraint (2.a) means that the lateral dimension of the aperture in the ferrite plate should not be too small in comparison to the internal lateral dimension of the winding. In fact, it is desirable to reduce the quantity of ferrite (thus the coils weight and cost) in the plate central region, wherein its presence is almost irrelevant on the self-inductance and coupling coefficient values [10]. The constraint (2.b) means that the ferrite plate width should not exceed too much the winding width. Lastly, the condition in (2.c) implies that the external lateral dimension of the winding should be sufficiently larger than the internal one, in order to avoid too thin windings and consequently higher losses. Applying constraints (2) to the previous parameter ranges of Table 1 leads to a significant reduction of the feasible test conditions: for each value of l_g, we eventually have 615 possible conditions that verify constraints (2). All these test conditions have been simulated by using Ansys Maxwell solver. The simulation time for a single run was about 1-3 minutes, on Intel Core i7-8700 CPU@3.20GHz, and 24.0 GB of RAM. The numerical FEM solver calculates the self and mutual inductance values over the given set of coils geometrical dimensions, and provides data sets to the GPA to generate analytical expressions of the inductance values, as a function of the geometrical parameters $Int_C, X_C, Int_W, X_W, l_g$.

It is worth noting that we calculate the inductance values only under alignment conditions of the IPT coils. In fact, the pads of Fig. 2 are intended for static IPT system. However, the proposed modeling approach is fully general and can be also implemented to search analytical expressions of the inductance values as a function of misalignment parameters. For instance, this approach is adopted in [14], where the mutual inductance value of a coil pair for an automotive

IPT system is derived as a function of the axial and lateral misalignments of the coils, and parametrized with respect to their reciprocal rotation angle. Therefore, in this paper we will only focus on analytical expressions that relate the self-inductance L and the mutual inductance M to geometrical design variables under perfect alignment conditions of the IPT coils.

III. SELF-INDUCTANCE AND MUTUAL INDUCTANCE BEHAVIORAL MODELING

In the design of an IPT system, the initial structure of the coil is mainly designed thanks to the intuition of experienced IPT designers [15]. After the initial design, an enhanced detailed design is normally realized through additional trials dedicated to simulations and experiments. This is the result of lack of formulas for the theoretical design of windings and ferrite core arrangement. This *trial-and-improve* approach is not just time-consuming, but it also prevents the achievement of a real optimization of the coils and of the overall IPT system. Enhanced machine-learning algorithms have been recently proposed in the literature, to support the optimal and innovative design of new coil pair structures [15], [16]. Unfortunately, these approaches do not provide analytical formulas that can enable coils characterization and optimization. Conversely, the availability of behavioral analytical models for the design of IPT links can be extremely helpful in the pre-design analysis and simulation phases of wireless charging systems.

The behavioral modeling approach has been recently demonstrated to be extremely helpful in both static and dynamic IPT system-level simulations. In [14], a behavioral analytical modeling of the mutual inductance of a coupled coil pair used in a static WPT system has been proposed. The paper also shows that it is possible to use the same behavioral model for modeling different coil pairs with the same shape (e.g., rectangular coils) but different dimensions and form factors. In fact, the model only differs in the formula coefficients, which can be tuned by means of a reduced training data set. Therefore, for coil pairs with a similar structure but different sizes, this kind of behavioral modeling can conveniently and reliably be adopted. This result is helpful in the case of scalable systems, where the designer can take the advantage of FEM simulations or experimental measurements executed on a small-size coil pair. Similarly, in [17] an analytical behavioral model for describing the mutual inductance between coupled coils in dynamic IPT systems is presented. The model is able to provide the variation of such a parameter assuming different trajectories of the vehicle. By using FEM simulation relevant to reciprocal positions between the coils, it was possible to build an analytical behavioral model able to retrieve the mutual inductance values along all the trajectories of interest.

In this paper, we propose new behavioral models of the self and mutual inductances for a square-shaped coil pair, as functions of their geometrical dimensions and reciprocal distance. These models can help in the analysis of scalable coil pairs and facilitate the final coil-pair design optimization. We achieve these results via a computational approach combining the results of an electromagnetic 3D-FEM numerical solver and a multi-objective evolutionary algorithm [18].

A. MULTI-OBJECTIVE GENETIC PROGRAMMING
Complex electromagnetic systems are often modeled using input-output data coming from experimental tests or FEM-based simulation results. Neural network modeling approach can be used for this purpose. Unfortunately, such method hides the analytical correlation among the parameters, the variables and the performances of the systems, and has other inherent disadvantages and limitations (e.g., decisions about the size and topology of the networks are needed, or a large amount of training and validation data could be required).

In this paper, the Genetic Programming Algorithm (GPA) is used for developing self and mutual inductance behavioral models from 3D-FEM simulations. The GPA performs symbolic regression and determines both the structure and the coefficients of the model during its evolution. As main advantage, no *a-priori* modeling assumptions are required.

The GPA has been largely used for chemical process modeling (e.g., for reactor systems [19]), for industrial production process (e.g., for fiber-to-yarn process [20]), and more recently for electronics systems modeling (e.g., for IGBTs [21], for power inductors [22] and power modules [23]). The scientific literature extensively describes the GPA [24] and its use in multi-objective evolutionary approach [25], [26]. Furthermore, several compiled codes, libraries and toolboxes have been released in the last decade (e.g., MATLAB case [27]). Accordingly, in this paper only a brief overview of the GPA is provided, as the main interest is not the method in itself to generate the behavioral models, but rather the use of behavioral models for design purposes. Therefore, comparisons neither to other evolutionary approaches nor to other existing tools will be performed.

The typical flowchart of the GPA is shown in [18]. The GPA works on a population of individuals (models), each one representing a potential solution to a problem. During its evolution, the GPA transforms the current population of models into a new population by applying the classical genetic operations (selection, cross-over, mutation, *etc.*). The GPA models are typically represented by means of tree structures. To construct such trees, the GPA considers a non-terminal set of elementary functions (herein, sum, multiplication, division, logarithm, arctangent, hyperbolic tangent, sine, exponential and power function have been used) and a terminal set composed of constant coefficients and input variables. Complexity factors (*cf*) have been assigned to all the elements included in these sets. For the elements of the terminal set we have considered $cf = 0.6$ for the input variables used in sum and multiplication operations and $cf = 1$ for the input variables used in all the other operations, and for constant

coefficients. For the non-terminal set we have adopted $cf = 1$ for sum and/or multiplication of elementary functions, $cf = 1.5$ for all the other functions. Beyond these elementary complexity factors, it is convenient to quantify the global complexity of each discovered GPA model. Thus, an overall complexity index ($F_{complexity}$) can be evaluated as follows: *if* a function is the argument of another function, *then* the complexity factors *cf* of the two functions are multiplied; *if* two functions are multiplied or summed, *then* their complexity factors *cf* are summed and subsequently multiplied by the complexity factor of a sum or a product.

In this paper, the multi-objective GPA is adopted to derive the self and the mutual inductance behavioral models valid for a square-shaped IPT coil pair. The self-inductance L and the mutual inductance M are modeled as explicit functions of the "variables" Int_W, X_W, X_C, and are parametrized with respect to "bias parameters" Int_C and l_g, as given in (3):

$$L = L_{bhv}\left(Int_W, X_W, X_C, \mathbf{p}\left(Int_C, l_g\right)\right) \quad (3.a)$$

$$M = M_{bhv}\left(Int_W, X_W, X_C, \mathbf{p}\left(Int_C, l_g\right)\right) \quad (3.b)$$

The bias parameters determine the numeric coefficient vector $\mathbf{p}\left(Int_C, l_g\right)$. The distinction in "variables" and "bias parameters" is dictated by the need of achieving a good tradeoff between complexity and accuracy of the behavioral models and making the GPA computational effort affordable. Indeed, it has been verified that it is quite difficult to get viable GPA solutions with more than three variables. Moreover, the measures Int_C and l_g have been chosen as bias parameters as they better ensure model coefficients monotonicity with respect to other possible choices of bias parameters (see Section III.B).

As first preliminary step, we have to select the test conditions to be simulated by the 3D-FEM numerical solver. For each test condition discussed in Section II, the FEM-based self and mutual inductance values, L_{FEM} and M_{FEM}, have been obtained and subsequently used to derive the analytical behavioral models, L_{bhv} and M_{bhv}. The Kennard and Stone's algorithm [28] has been adopted to obtain a separation of the FEM-based data into a training data set T (used to derive the behavioral models) and a validation data set V (used to evaluate the models generalization capability). The training data set T consists of 960 total test conditions (320 conditions for each l_g), whereas the validation data set V includes 885 total conditions (295 conditions for each l_g). For a detailed description of the behavioral modeling approach, let us refer to the GPA implemented to discover the analytical function of L_{bhv}. Similar considerations hold for M_{bhv}. A set of m_1 values of $Int_{C,j1}$ has been considered, with $j_1 = 1, \ldots, m_1$, and a set of m_2 values of $l_{g,j2}$ has been analyzed, with $j_2 = 1, \ldots, m_2$, thus resulting in the overall $m = m_1 \times m_2$ geometrical conditions $(Int_{C,j}, l_{g,j})$, with $j = 1, \ldots, m$. For each condition, n combinations of $(Int_{W,i}, X_{W,i}, X_{C,i})$ have been considered, with $i = 1, \ldots, n$. For each of the resulting $n \times m$ test conditions, a data vector has been defined, including the test values $(Int_{W,i}, X_{W,i}, X_{C,i}, Int_{C,j}, l_{g,j})$ and the resultant self-inductance value $L_{ij} = L_{FEM}$

$(Int_{W,i}, X_{W,i}, X_{C,i}, Int_{C,j}, l_{g,j})$, simulated by means of Ansys Maxwell. Herein, we have adopted $m_1 = 4$, $m_2 = 3$, $n = 80$, resulting in the $n \times m = 960$ total test conditions of the training data set T. The GPA has to identify the behavioral model L_{bhv} such that the value of this function – computed for each test condition of the training data set T – is as close as possible to the corresponding training value L_{ij}, $\forall i \in \{1, \ldots, n\}$ and $\forall j \in \{1, \ldots, m\}$. The structure of the function L_{bhv} must be the same for all the values of $Int_{C,j}$ and l_{gj} $\forall j \in \{1, \ldots, m\}$, while the coefficients $\mathbf{p}$ are functions of Int_C and l_g and can vary with them. To determine such coefficients for each (Int_C, l_g) condition, a Non-Linear Least Squares (NLLS) algorithm, based on the Levenberg-Marquardt optimization method [29], has been applied to the respective n data vectors. Thus, the values of the coefficients $\mathbf{p}$ have been determined by minimizing the χ-squared error between the FEM-based values L_{ij} and the GPA-predicted values L_{bhv} ($Int_{W,i}$, $X_{W,i}$, $X_{C,i}$, $\mathbf{p}$ $(Int_{C,j}, l_{g,j})$) $\forall i \in \{1, \ldots, n\}$, as given in (4):

$$\chi_j^2 = \frac{1}{n}\sum_{i=1}^{n}\left\{100\,\frac{L_{bhv}\left(Int_{Wi}, X_{Wi}, X_{Ci}, \mathbf{p}\left(Int_{Cj}, l_{gj}\right)\right) - L_{ij}}{L_{ij}}\right\}^2 \quad (4)$$

Interpolating functions of $\mathbf{p}$ $(Int_{C,j}, l_{g,j})$ can be determined, as discussed in next paragraph. Finally, an elitist Non-dominated Sorting Genetic Algorithm (NSGA-II, [25]) can be adopted to discover the L_{bhv} models (and similarly, the M_{bhv} models) ensuring optimal trade-off between "complexity" and "accuracy", selected as objective functions for minimization in this multi-objective optimization problem. The model complexity, namely the previously introduced $F_{complexity}$ index, is the result of the complexity factors of the elementary functions adopted in the model structure. The model accuracy index, $F_{accuracy}$, can be estimated by means of the Root Mean Square Error (*RMSE*) between the FEM-based values and the GPA-predicted values over the whole training data set:

$$RMSE = \sqrt{\frac{1}{m}\sum_{j=1}^{m}\chi_j^2} \quad (5)$$

B. MODELING RESULTS AND DISCUSSION

The multi-objective GPA has been executed over 50 runs, with a population of 500 models evolving over 300 generations for each run. The simulation time for a single run was about 1 h on an Intel Core i7-6500U processor. It is worth clarifying that the proposed modeling approach is intended to discover a behavioral model, namely an analytical formula. Once the behavioral model is identified, the final user does not need to perform additional runs of the multi-objective GPA, because the same model formula can be adopted for similar coil pair geometries, whereas the model coefficient values can be tuned starting from relevant training data set. Hence, the use of the discovered analytical formula significantly reduces the computation times, if compared to FEM simulations.

Each GPA model has been scored on the basis of the following metrics:

- N_{run}: the number of runs during which the algorithm has discovered the model;
- N_{gen}: the average number of generations during which the model survived in the population;
- $err_{T,max}$: the maximum value of the model percent error over the training data set T;
- $err_{V,max}$: the maximum value of the model percent error over the validation data set V;
- N_{mon}: the average number of intervals over which the model coefficients p change their monotonicity with Int_C and l_g.

The best models are the ones maximizing the first two metrics and minimizing the last three metrics. Only the non-dominated Pareto-optimal solutions occurring in at least $N_{run} = 2$ runs, with the maximum training set percent error $err_{T,max}$ lower than 11%, with $F_{complexity}$ lower than 9 and with regular monotonous coefficient trends ($N_{mon} = 1$) have been considered for further comparison. Such GPA solutions are listed in Table 2, where the models have been sorted based on their complexity (simpler formulas in the bottom part of the table). Table 3 provides their respective metrics values. The solution given in bold in Tables 2-3 presents a good trade-off among the accuracy ($RMSE = 2.4\%$, with $err_{T,max} = 9.8\%$ and $err_{V,max} = 10.4\%$), complexity ($F_{complexity} = 6.5$) and repeatability ($N_{run} = 19$), and has been selected as a reference self-inductance behavioral model for the analyzed dataset. This solution has been re-written in (6):

$$L_{bhv} = \alpha_0 X_C + \alpha_1 X_W \sqrt{X_C} + Int_W (\alpha_2 + \alpha_3 X_W + \alpha_4 X_C) \tag{6}$$

As further improvement of the performed modeling, we have also tested the discovered model (6) over an extended air-gap range, including the values $l_g = \{70, 90\}$ mm outside the original range used for modeling, the other test conditions being unchanged. More precisely, the values of the model coefficients α_i ($i = 0, \ldots, 4$) for such new air gap values have been obtained by applying the NLLS algorithm, with the same fitting procedure used to obtain the coefficient values for $l_g = \{10, 30, 50\}$ mm. All the coefficients present quite regular trends and can be well approximated by a third-order polynomial function of Int_C (see Eq. (7)), whose fitting coefficients β_j ($j = 0, \ldots, 3$) change with the air gap and can be approximated by a fourth-order polynomial function of l_g (see Eq. (8)):

$$\alpha_i = \beta_0 Int_C^3 + \beta_1 Int_C^2 + \beta_2 Int_C + \beta_3 \tag{7}$$
$$\beta_j = \gamma_0 l_g^4 + \gamma_1 l_g^3 + \gamma_2 l_g^2 + \gamma_3 l_g + \gamma_4 \tag{8}$$

The resulting fitting coefficients γ_k are listed in Table 4. All the geometrical dimensions in the self-inductance model (6)-(8) are expressed in mm, while L_{bhv} is given in μH.

For all the test conditions included in the training and validation data sets for the five tested air gap values $l_g = \{10, 30, 50, 70, 90\}$ mm, the percent errors between the self-inductance model predictions and FEM-based data are very low and always limited in the range of about $\pm 13\%$, as depicted in Fig. 3. Let us note that the test conditions given

TABLE 2. Models discovered by multi-objective GPA.

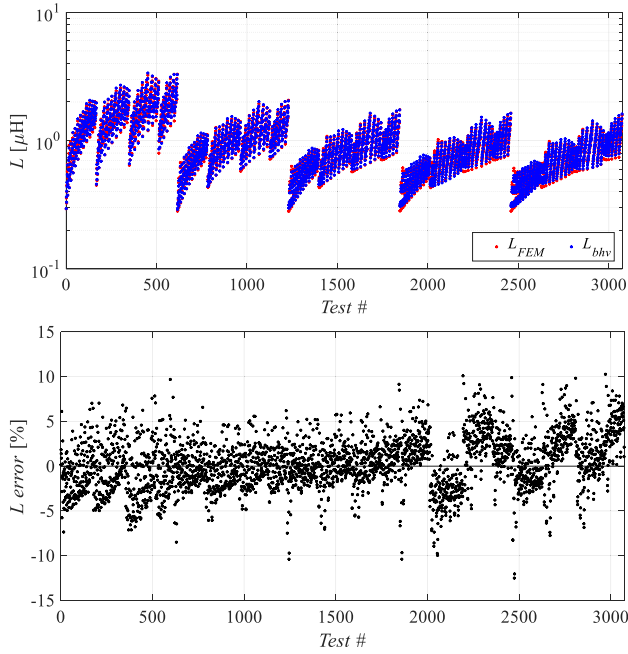| Model	Expression for L_{bhv}
#1	$\alpha_0(X_W^2)X_W + \alpha_1 X_W X_C + \alpha_2 Int_W + \alpha_3 X_C Int_W + \alpha_4 Int_W X_W + \alpha_5 X_C^2 + \alpha_6 X_C$
#2	$\alpha_0 X_C + \alpha_1 Int_W + \alpha_2 (X_C^2) Int_W + \alpha_3 X_C X_W + \alpha_4 Int_W X_W + \alpha_5 X_C Int_W + \alpha_6 X_W$
#3	$\alpha_0 Int_W X_W + \alpha_1 X_C X_W + \alpha_2 Int_W X_C + \alpha_3 Int_W + \alpha_4 \sqrt{(X_C)} + \alpha_5 X_C^2 + \alpha_6 X_W$
#4	$\alpha_0 Int_W X_W + \alpha_1 X_C X_W + \alpha_2 (X_C(\exp(\alpha_3 X_C)))(1/X_W) + \alpha_4 Int_W + \alpha_5 X_C Int_W$
#5	$\alpha_0 Int_W X_W + \alpha_1 Int_W X_C + \alpha_2 X_C (1/X_W) + \alpha_3 Int_W + \alpha_4 X_C^2 + \alpha_5 X_C X_W$
#6	$\alpha_0 X_C X_W + \alpha_1 X_W + \alpha_2 Int_W X_C + \alpha_3 Int_W X_W + \alpha_4 X_C + \alpha_5(\sqrt{(X_C)})Int_W$
#7	$\alpha_0 X_C + \alpha_1 X_C Int_W + \alpha_2 X_C^2 + \alpha_3 Int_W X_W + \alpha_4 X_C (\sqrt{(X_W)}) + \alpha_5 Int_W$
#8	$\alpha_0 Int_W + \alpha_1 X_C Int_W + \alpha_2 X_W Int_W + \alpha_3 X_C X_W + \alpha_4 (\exp(\alpha_5 X_W))(\exp(\alpha_6 X_C))$
#9	$\alpha_0(\sqrt{(X_C)})X_W + \alpha_1 X_W + \alpha_2 Int_W + \alpha_3 Int_W X_W + \alpha_4 X_C + \alpha_5 Int_W X_C$
#10	$\boldsymbol{\alpha_0 X_C + \alpha_1 X_W \sqrt{(X_C)} + Int_W(\alpha_2 + \alpha_3 X_W + \alpha_4 X_C)}$
#11	$\alpha_0(\sqrt{(\alpha_1 X_C)})X_W + \alpha_2 Int_W + \alpha_3 Int_W X_W + \alpha_4 X_C + \alpha_5 X_C Int_W$
#12	$\alpha_0(Int_W + \alpha_1 \sqrt{(\alpha_2 X_C)})X_W + \alpha_3 X_C + \alpha_4 Int_W + \alpha_5 X_C Int_W$
#13	$\alpha_0 X_W Int_W + \alpha_1 X_W^2 + \alpha_2 Int_W + \alpha_3 Int_W X_C + \alpha_4 X_C / X_W$

TABLE 3. Metrics values for models listed in Table 2 ($N_{mon} = 1$).

Model	RMSE [%]	$F_{complexity}$	N_{run}	N_{gen}	$err_{T,max}$ [%]	$err_{V,max}$ [%]
#1	1.6	8.6	11	118	9.4	10
#2	2.1	8.4	7	165	10.1	9
#3	2.1	8.3	2	179	10.8	9
#4	1.7	8.2	2	19	8.9	9.1
#5	1.9	7.9	2	135	8.5	8.9
#6	2.2	7.7	2	151	8.9	8.5
#7	1.9	7.7	5	111	8.7	9.1
#8	1.5	7.6	3	96	8	8.3
#9	2.3	7.5	5	115	9.9	9.9
#10	**2.4**	**6.5**	**19**	**131**	**9.8**	**10.4**
#11	2.4	6.5	8	153	9.8	10.4
#12	2.4	6.3	2	215	9.8	10.4
#13	2.7	6.1	2	37	11	9.4

TABLE 4. Coefficients of the self-inductance model (6)-(8).

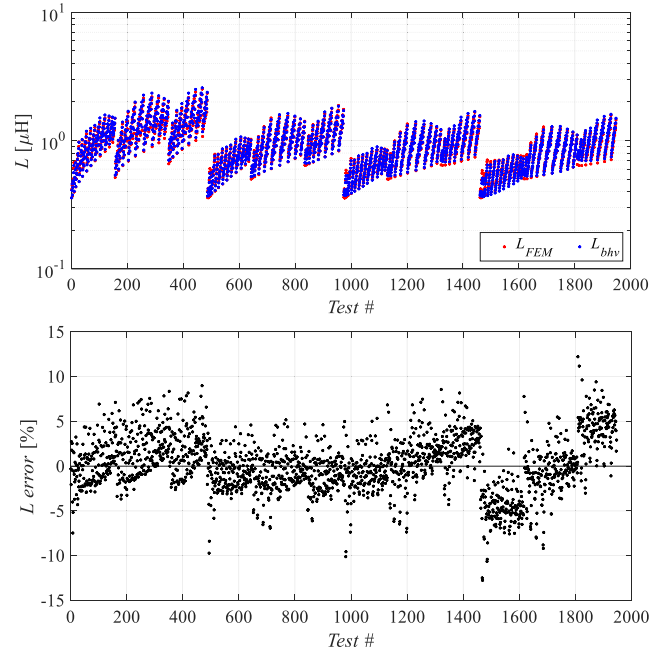| Coeffs.		γ_0	γ_1	γ_2	γ_3	γ_4
α_0	β_0	4.84E-16	-8.66E-14	4.08E-12	4.21E-11	-4.73E-09
	β_1	-2.95E-13	6.01E-11	-3.95E-09	7.65E-08	2.37E-07
	β_2	4.52E-11	-9.46E-09	6.59E-07	-1.54E-05	3.64E-05
	β_3	-2.07E-09	4.40E-07	-3.17E-05	8.29E-04	-5.92E-03
α_1	β_0	-7.29E-18	1.78E-15	-1.07E-13	-1.95E-12	1.91E-10
	β_1	6.47E-15	-1.74E-12	1.48E-10	-3.84E-09	7.61E-09
	β_2	-1.01E-12	2.83E-10	-2.56E-08	7.84E-07	-5.33E-06
	β_3	4.70E-11	-1.37E-08	1.31E-06	-4.57E-05	5.86E-04
α_2	β_0	4.84E-17	-9.13E-15	7.65E-13	-7.28E-11	2.35E-09
	β_1	1.46E-14	-7.23E-12	9.27E-10	-2.95E-08	2.36E-07
	β_2	-2.96E-12	1.47E-09	-1.96E-07	7.90E-06	-1.09E-04
	β_3	-1.90E-11	-3.43E-08	6.45E-06	-2.86E-04	8.32E-03
α_3	β_0	3.59E-18	-7.82E-16	5.92E-14	-1.69E-12	1.46E-11
	β_1	-1.88E-15	4.28E-13	-3.46E-11	1.13E-09	-1.37E-08
	β_2	2.76E-13	-6.37E-11	5.26E-09	-1.79E-07	2.33E-06
	β_3	-1.33E-11	3.15E-09	-2.70E-07	9.97E-06	-1.70E-04
α_4	β_0	-1.33E-18	2.92E-16	-2.22E-14	6.31E-13	-5.36E-12
	β_1	6.93E-16	-1.62E-13	1.34E-11	-4.50E-10	5.76E-09
	β_2	-9.59E-14	2.30E-11	-1.98E-09	7.00E-08	-9.35E-07
	β_3	6.38E-12	-1.61E-09	1.49E-07	-6.16E-06	1.18E-04

FIGURE 3. Predictions of the behavioral model (6)-(8) over training and validation data set: (top) self-inductance values obtained by FEM simulations (red markers) and predicted by the model (6)-(8) (blue markers); (bottom) relative percent errors.

FIGURE 4. Predictions of the behavioral model (6)-(8) over additional validation data set: (top) self-inductance values obtained by FEM simulations (red markers) and predicted by the model (6)-(8) (blue markers); (bottom) relative percent errors.

along the x-axis have been sorted first in the ascending order of l_g, then of Int_C, X_W, Int_W and, finally, of X_C.

We have further validated the discovered self-inductance model (6) by proving the generalization capability of the model coefficient laws given in (7) and (8). An additional validation data set has been introduced, assembled with the following values: $l_g = \{20, 40, 60, 80\}$ mm and $Int_C = \{110, 160, 210\}$ mm, different from the original values $l_g = \{10, 30, 50, 70, 90\}$ mm and $Int_C = \{85, 135, 185, 235\}$ mm used to generate the model coefficients. The values of the remaining parameters $\{Int_W, X_W, X_C\}$ remain the ones comprised in the ranges of Table 1 and satisfying the feasibility constraints (2). For all the considered validation test conditions, the percent errors of the model (6)-(8) are very low, with the maximum percent error of 12.2%, as depicted in Fig. 4. This result confirms the fact that the proposed behavioral model generalizes well the coefficient trends with respect to both l_g and Int_C. Hence, the discovered model (6)-(8) can be reliably applied to evaluate the self-inductance of the square-shaped coils over the entire range of $l_g = [10, 90]$ mm and $Int_C = [85, 235]$ mm, while the ranges of the other parameters (Int_W, X_W, X_C) can be easily evaluated by means of the introduced feasibility constraints (2).

Similarly, the GPA has been set up to discover the analytical function of M_{bhv}. The same set of m geometrical conditions $(Int_{C,j}, l_{g,j})$, with $j = 1, \ldots, m$, has been considered. For each condition, n combinations of $(Int_{W,i}, X_{W,i}, X_{C,i})$ have been used, with $i = 1, \ldots, n$. For each of the resulting $n \times m$ test conditions, a data vector has been defined, including

the test values $(Int_{W,i}, X_{W,i}, X_{C,i}, Int_{C,j}, l_{g,j})$ and the mutual inductance values $M_{ij} = M_{FEM}(Int_{W,i}, X_{W,i}, X_{C,i}, Int_{C,j}, l_{g,j})$, simulated by means of Ansys Maxwell. The GPA has to identify the behavioral model M_{bhv} such that the value of this function – computed for each test condition of the training data set T – is as close as possible to the corresponding training value M_{ij}, $\forall i \in \{1, \ldots, n\}$ and $\forall j \in \{1, \ldots, m\}$. According to previous metrics, the solution for the mutual inductance behavioral model is given in (9):

$$M_{bhv} = \rho_0 X_C + \rho_1 X_W + \rho_2 Int_W \\ + X_C^2 \left[\rho_3 + \rho_4 (Int_W X_W)^{-1} \right] \quad (9)$$

where the interpolating functions (10)-(11) have been used to define the model coefficients as functions of Int_C and l_g:

$$\rho_i = \lambda_0 Int_C^3 + \lambda_1 Int_C^2 + \lambda_2 Int_C + \lambda_3 \quad (10)$$
$$\lambda_j = \delta_0 l_g^4 + \delta_1 l_g^3 + \delta_2 l_g^2 + \delta_3 l_g + \delta_4 \quad (11)$$

for $i = 0, \ldots, 4$ and $j = 0, \ldots, 3$. The resulting fitting coefficients δ_k are listed in Table 5. All the geometrical dimensions in the mutual inductance model (9)-(11) are expressed in mm, while M_{bhv} is given in μH.

Fig. 5 compares the predictions of the mutual inductance model (9)-(11) with the FEM-based data, for all the test conditions included in the training and validation data sets for the five tested air-gap values $l_g = \{10, 30, 50, 70, 90\}$ mm. The percent errors are quite low and limited in the range of about $\pm 13\%$. Eventually, Fig. 6 shows the mutual inductance fittings and percent errors with respect to the FEM-based data
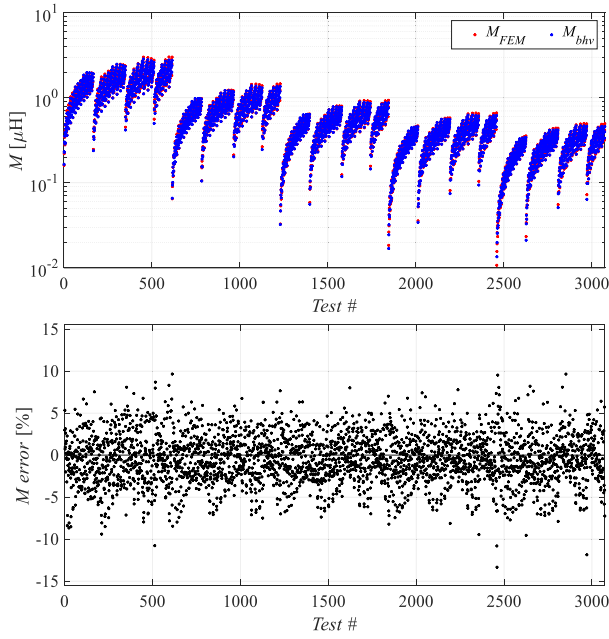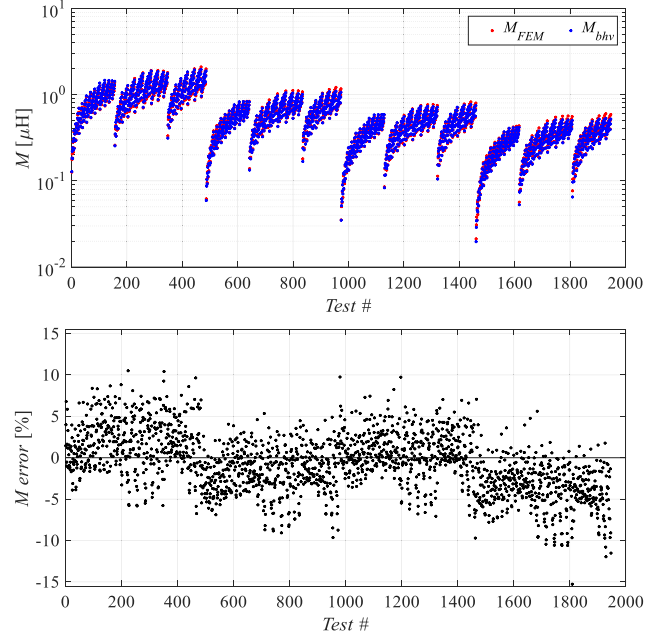
FIGURE 5. Predictions of the behavioral model (9)-(11) over training and validation data set: (top) mutual inductance values obtained by FEM simulations (red markers) and predicted by the model (9)-(11) (blue markers); (bottom) relative percent errors.
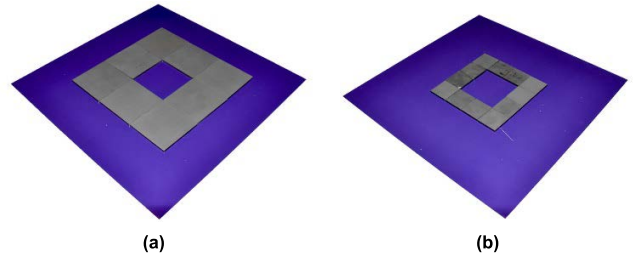

FIGURE 6. Predictions of the behavioral model (9)-(11) over additional validation data set: (top) mutual inductance values obtained by FEM simulations (red markers) and predicted by the model (9)-(11) (blue markers); (bottom) relative percent errors.

TABLE 5. Coefficients of the mutual inductance model (9)-(11).

Coeffs.		δ_0	δ_1	δ_2	δ_3	δ_4
ρ_0	λ_0	-3.55E-16	8.86E-14	-7.38E-12	2.32E-10	-2.02E-09
	λ_1	2.36E-13	-5.87E-11	5.05E-09	-1.76E-07	2.16E-06
	λ_2	-3.40E-11	8.38E-09	-7.11E-07	2.37E-05	-2.41E-04
	λ_3	1.81E-09	-4.47E-07	3.87E-05	-1.39E-03	1.83E-02
ρ_1	λ_0	1.31E-16	-3.39E-14	3.01E-12	-1.09E-10	1.50E-09
	λ_1	-8.22E-14	2.09E-11	-1.86E-09	6.94E-08	-1.01E-06
	λ_2	1.05E-11	-2.61E-09	2.24E-07	-7.59E-06	7.95E-05
	λ_3	-6.09E-10	1.52E-07	-1.33E-05	4.83E-04	-6.20E-03
ρ_2	λ_0	1.30E-16	-3.19E-14	2.52E-12	-6.63E-11	3.79E-10
	λ_1	-8.15E-14	2.02E-11	-1.68E-09	5.32E-08	-6.18E-07
	λ_2	1.21E-11	-2.99E-09	2.51E-07	-8.06E-06	9.41E-05
	λ_3	-5.05E-10	1.24E-07	-1.04E-05	3.44E-04	-5.04E-03
ρ_3	λ_0	1.18E-19	-3.61E-17	3.55E-15	-1.35E-13	1.76E-12
	λ_1	-1.02E-16	2.84E-14	-2.71E-12	1.06E-10	-1.59E-09
	λ_2	1.87E-14	-5.02E-12	4.71E-10	-1.84E-08	2.78E-07
	λ_3	-7.53E-13	2.00E-10	-1.85E-08	7.07E-07	-9.56E-06
ρ_4	λ_0	1.00E-14	-1.88E-12	6.22E-11	4.45E-09	-2.29E-07
	λ_1	-1.04E-11	2.34E-09	-1.69E-07	4.18E-06	-2.11E-05
	λ_2	1.55E-09	-3.48E-07	2.53E-05	-6.12E-04	1.50E-03
	λ_3	-7.41E-08	1.68E-05	-1.25E-03	3.30E-02	-1.86E-01

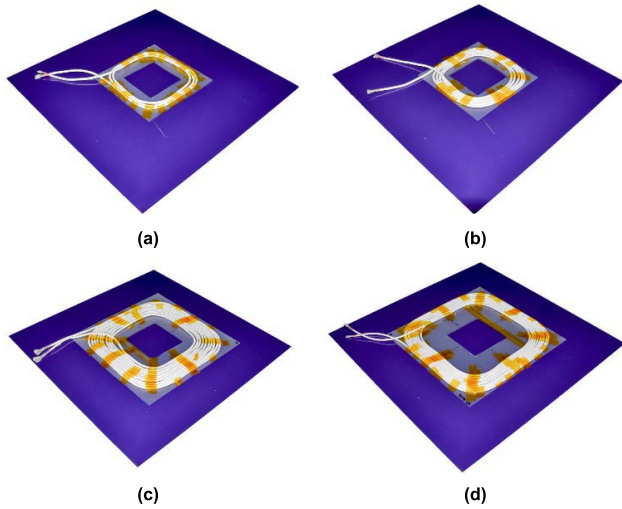**FIGURE 7.** The magnetic core built to validate the behavioral modeling formulas: (a) C1 and (b) C2.

IV. EXPERIMENTAL VALIDATION

In this Section, the experimental validation of the discovered behavioral modeling formulas is presented. IPT link prototypes, each one composed of two identical coils, are built for validation, by combining two magnetic ferrite cores and four winding arrangements. The magnetic tile ferritelinks employed for the magnetic core are made of the 3C95 material from Ferroxcube [30]. The two cores **C1** and **C2** depicted in Fig. 7 are realized as follows.

C1. The core shown in Fig. 7(a) is composed of 8 tiles of 100 mm × 100 mm × 5 mm, and the parameters of reference are $X_C = 300$ mm and $Int_C = 100$ mm.

C2. The core shown in Fig. 7(b) is composed of 12 tiles of 50 mm × 50 mm × 5 mm, and the parameters of reference are $X_C = 200$ mm and $Int_C = 100$ mm.

The windings are realized by Litz-wire from Masfarne [31]. The four proposed windings **W1**, **W2**, **W3** and **W4** depicted in Fig. 8 are realized as follows.

over the additional validation data set described previously (including the test conditions for $l_g = \{20, 40, 60, 80\}$ mm and $Int_C = \{110, 160, 210\}$ mm). Limited prediction errors (within ±15%) prove a good generalization capability of the mutual inductance behavioral model (9)-(11).
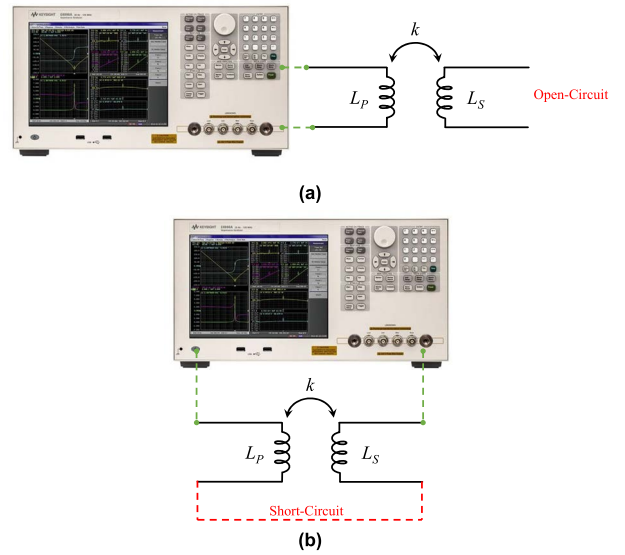
FIGURE 8. The windings arranged to validate the behavioral modeling formulas: (a) W1, (b) W2, (c) W3 and (d) W4.

FIGURE 9. Experimental measuring setup to obtain (a) the self-inductance and (b) the coupling factor measurement of an IPT link.

W1. The winding shown in Fig. 8(a) has 3 turns in series, and the parameters of reference are $X_W = 180$ mm and $Int_W = 140$ mm. The litz-wire employed is 3000 strands and 0.07 mm diameter.

W2. The winding shown in Fig. 8(b) has 5 turns in series, and the parameters of reference are $X_W = 190$ mm and $Int_W = 135$ mm. The litz-wire employed is 3000 strands and 0.07 mm diameter.

W3. The winding shown in Fig. 8(c) has 10 turns in series, and the parameters of reference are $X_W = 275$ mm and $Int_W = 165$ mm. The litz-wire employed is 3000 strands and 0.07 mm diameter.

W4. This winding shown in Fig. 8(d) has 10 turns in series, and the main parameters of reference are $X_W = 290$ mm and $Int_W = 210$ mm. The litz-wire employed is 1000 strands and 0.2 mm diameter.

The following IPT link prototypes have been considered: **C1-W1, C1-W2, C1-W3, C1-W4, C2-W1,** and **C2-W2**, where the air gap between primary and secondary has been varied according to the following values: 10 mm, 30 mm, 50 mm, and 80 mm. Given the geometries, it was impossible to have the combinations **C2-W3** and **C2-W4** (being $X_C < X_W$).

As first preliminary validation, we proved the accuracy of the FEM-based data obtained for the built IPT link prototypes against the experimental measurements of the resultant self-inductance and mutual inductance values. Experimental measurements have been performed by using the Keysight E4990A impedance analyzer. The methodology to obtain the experimental measurement is as follows: the primary-side self-inductance L_P has been obtained by measuring the input impedance at the primary terminals with the secondary coil in open circuit, as shown in Fig. 9(a). Similarly, the secondary-side self-inductance L_S has been measured. The mutual inductance and coupling factor measurements are

obtained by connecting one terminal of primary-side and one terminal of the secondary-side to the impedance analyzer, then measuring the input impedance when the other two terminals are connected together, as shown in Fig 9(b). Thus, we can measure the total equivalent inductance as:

$$L_K = L_P(1 - k) + L_S(1 - k) \qquad (12)$$

Then, from the previous measurements, we can obtain the coupling factor as given in (13):

$$k = 1 - \frac{L_K}{L_P + L_S} \qquad (13)$$

Finally, the mutual inductance M can be expressed as a function of k, L_P and L_S, as given in (1).

Measurements, FEM simulations and the results obtained from the behavioral models given in (6) and (9) are compared in Fig. 10 to Fig. 15. On the x-axis, the details of the prototype and tested air gap are provided. The descriptor "lgx", with $x = [1; 3; 5; 8]$, represents the air-gap length: $lg1 = 10$ mm, $lg3 = 30$ mm, $lg5 = 50$ mm, $lg8 = 80$ mm. On the y-axis, one can visualize the self-inductance, the mutual-inductance and the coupling factor of the IPT link.

At first, the accuracy of the FEM data is experimentally verified. Fig. 10, Fig. 11, and Fig. 12 show the comparison between the FEM-based simulation results and the experimental measurements for the self-inductance, mutual-inductance and coupling factor values and the resulting percent errors. For all the cases, the percent error is always included in ±30% range (for most cases, strictly included within ±15%). From Fig. 10 one can notice that the worst cases occur when the IPT coils are in the closest position. This is due to the sensitivity of this coefficient to the air gap distance when it is quite small with respect to the IPT coil area. The sharp change from 10 mm to 30 mm can
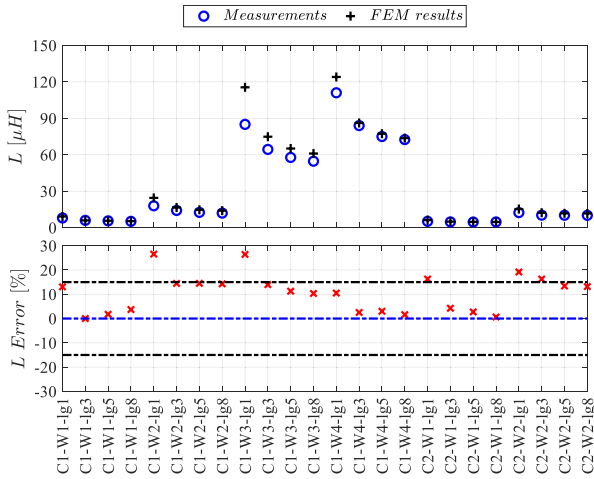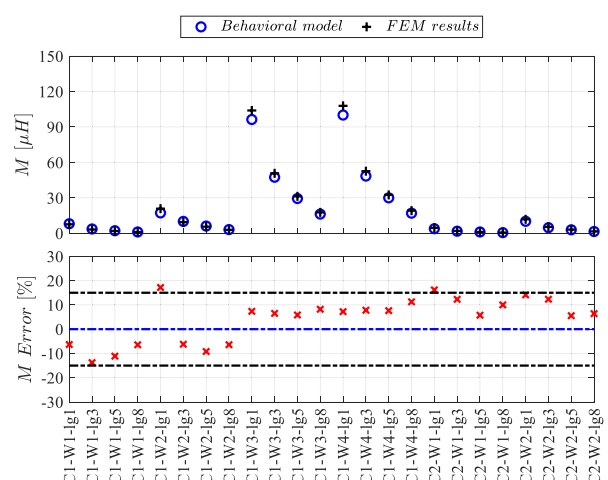
FIGURE 10. Comparison of experimental measurements versus FEM simulation results of the self-inductance.
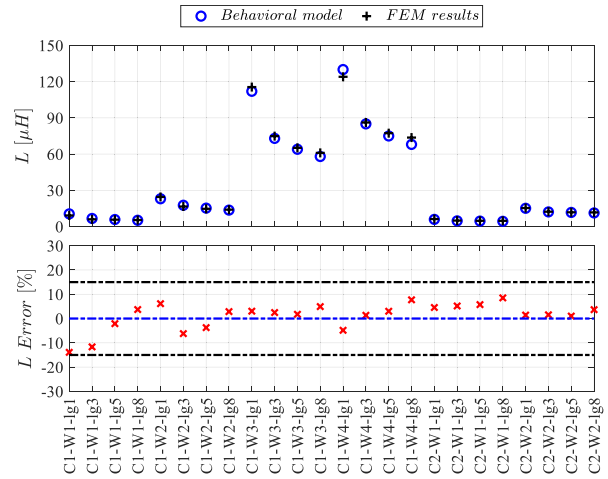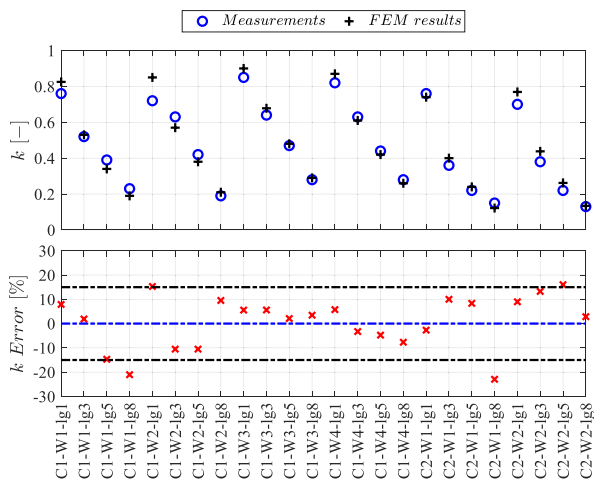

FIGURE 13. Comparison of behavioral model results versus FEM simulation results of the self-inductance.
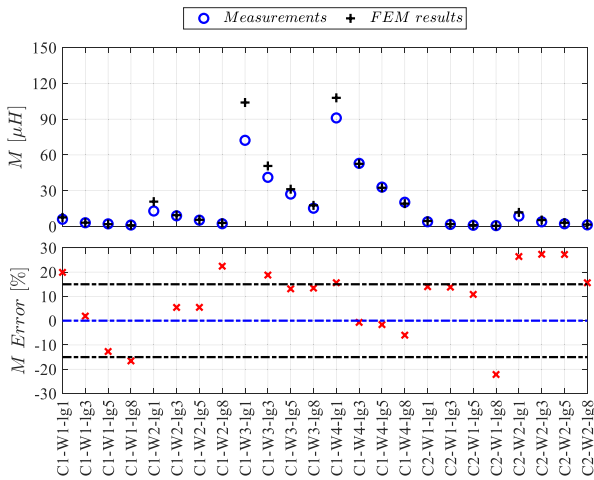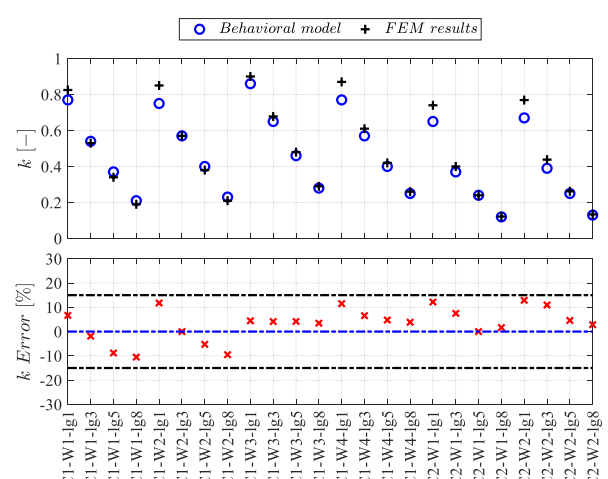

FIGURE 11. Comparison of experimental measurements versus FEM simulation results of the mutual inductance.

FIGURE 14. Comparison of behavioral model results versus FEM simulation results of the mutual inductance.

FIGURE 12. Comparison of experimental measurements versus FEM simulation results of the coupling factor.

FIGURE 15. Comparison of behavioral model results versus FEM simulation results of the coupling factor.

be seen in the inductance value. Similar considerations are valid for the mutual inductance values compared in Fig. 11. Finally, from Fig. 12 one can notice that most of the cases are

within ±15% (only two cases at the largest distance present errors around 20%, which still remain acceptable in IPT coils design context). Overall, the accuracy of the FEM-based data

obtained for the built IPT link prototypes is proved against experimental measurements.

Finally, the predictions of self-inductance, mutual inductance and coupling factor values have been compared to the FEM-based data, as shown in Fig. 13, Fig. 14, and Fig. 15 with the resulting percent errors. From this comparison, we can see that for all the case studies the self-inductance, mutual inductance and coupling factor errors are within ±15%, and for the majority of cases strictly included within ±10% (in agreement with the percent errors evaluated in Section III), thus corroborating the good accuracy of the behavioral models and the valued chance of using these formulas to design IPT links without using FEM simulations.

V. CONCLUSION

The adoption of behavioral models for Inductive Power Transfer (IPT) coil pairs can considerably reduce the time and computational costs of IPT systems design. Novel analytical formulas for the evaluation of the self-inductance and mutual inductance values are proposed in this work. A multi-objective genetic programming algorithm has been adopted to generate these behavioral models for coil pairs, by taking into account the geometric parameters defining the IPT link. The behavioral modeling predictions have been compared with finite element results and experimental data, showing a good accuracy and generalization capability. The adoption of these formulas for the design of IPT links can overcome the iterative design process normally realized in finite element tools, thus reducing time and computational resources.

REFERENCES

[1] X. Qu, Y. Jing, H. Han, S.-C. Wong, and C. K. Tse, "Higher order compensation for inductive-power-transfer converters with constant-voltage or constant-current output combating transformer parameter constraints," *IEEE Trans. Power Electron.*, vol. 32, no. 1, pp. 394–405, Jan. 2017.

[2] A. Delgado, N. A. Requena, R. Ramos, J. A. Oliver, P. Alou, and J. A. Cobos, "Design of inductive power transfer system with a behavior of voltage source in open-loop considering wide mutual inductance variation," *IEEE Trans. Power Electron.*, vol. 35, no. 11, pp. 11453–11462, Nov. 2020.

[3] W. Zhang and C. C. Mi, "Compensation topologies of high-power wireless power transfer systems," *IEEE Trans. Veh. Technol.*, vol. 65, no. 6, pp. 4768–4778, Jun. 2016.

[4] S. Li, W. Li, J. Deng, T. D. Nguyen, and C. C. Mi, "A double-sided LCC compensation network and its tuning method for wireless power transfer," *IEEE Trans. Veh. Technol.*, vol. 64, no. 6, pp. 2261–2273, Jun. 2015.

[5] S. Jayalath and A. Khan, "Design, challenges, and trends of inductive power transfer couplers for electric vehicles: A review," *IEEE J. Emerg. Sel. Topics Power Electron.*, vol. 9, no. 5, pp. 6196–6218, Oct. 2021.

[6] E. B. Rosa and F. W. Grover, "Formulas and tables for the calculation of mutual and self-inductance," *J. Washington Acad. Sci.*, vol. 1, pp. 14–16, Jul. 1911.

[7] A. Delgado, D. Schoenberger, J. A. Oliver, P. Alou, and J. A. Cobos, "Design guidelines of inductive coils using a polymer bonded magnetic composite for inductive power transfer systems in electric vehicles," *IEEE Trans. Power Electron.*, vol. 35, no. 8, pp. 7884–7893, Aug. 2020.

[8] M. S. Carmeli, F. Castelli-Dezza, M. Mauri, and G. Foglia, "Contactless energy transmission system for electrical vehicles batteries charging," in *Proc. Int. Conf. Clean Electr. Power (ICCEP)*, Taormina, Italy, Jun. 2015, pp. 499–505.

[9] Y. Zhang, L. Wang, Y. Guo, and C. Tao, "Design and optimization of asymmetrical spiral rectangular pads for EV wireless charging," in *Proc. IEEE 4th Southern Power Electron. Conf. (SPEC)*, Singapore, Dec. 2018, pp. 1–5.

[10] P. S. R. Nayak and D. Kishan, "Design and analysis of SS resonant IPT system with computed mutual inductance through FEM model," in *Proc. Int. Conf. Power, Instrum., Control Comput. (PICC)*, Thrissur, India, Jan. 2018, pp. 1–5.

[11] A. Delgado, G. Salinas, J. A. Oliver, J. A. Cobos, and J. Rodriguez-Moreno, "Equivalent conductor layer for fast 3-D finite element simulations of inductive power transfer coils," *IEEE Trans. Power Electron.*, vol. 35, no. 6, pp. 6221–6230, Jun. 2020.

[12] *Wireless Power Transfer for Light-Duty Plug-In EVs and Alignment Methodology*, document J2954, SAE, May 2016.

[13] *Ansys Maxwell*. Accessed: Oct. 10, 2021. [Online]. Available: https://www.ansys.com/products/electronics/ansys-maxwell

[14] G. Di Capua, N. Femia, K. Stoyka, G. Di Mambro, A. Maffucci, S. Ventre, and F. Villone, "Mutual inductance behavioral modeling for wireless power transfer system coils," *IEEE Trans. Ind. Electron.*, vol. 68, pp. 2196–2206, Mar. 2021.

[15] B. Choi and Y. S. Kim, "New structure design of ferrite cores for wireless EV charging by machine learning," *IEEE Trans. Ind. Electron.*, vol. 68, no. 12, pp. 12162–12172, Dec. 2021.

[16] B. Choi, E. S. Lee, and Y. S. Kim, "Optimal structure design of ferromagnetic cores in wireless power transfer by reinforcement learning," *IEEE Access*, vol. 8, pp. 179295–179306, 2020.

[17] G. Di Capua, A. Maffucci, K. Stoyka, G. Di Mambro, S. Ventre, V. Cirimele, F. Freschi, F. Villone, and N. Femia, "Analysis of dynamic wireless power transfer systems based on behavioral modeling of mutual inductance," *Sustainability*, vol. 13, p. 2556, Feb. 2021.

[18] M. J. Willis, H. G. Hiden, P. Marenbach, B. McKay, and G. A. Montague, "Genetic programming: An introduction and survey of applications," in *Proc. 2nd Int. Conf. Genetic Algorithms Eng. Syst., Innov. Appl.*, Glasgow, U.K., Sep. 1997, pp. 314–319.

[19] B. McKay, M. Willis, and G. Barton, "Steady-state modelling of chemical process systems using genetic programming," *Comput. Chem. Eng.*, vol. 21, no. 9, pp. 981–996, 1997.

[20] S. Sette and L. Boullart, "Genetic programming: Principles and applications," *Eng. Appl. Artif. Intell.*, vol. 14, no. 6, pp. 727–736, 2001.

[21] N. Femia, M. Migliaro, and A. D. Cioppa, "A genetic programming approach to modeling power losses of Insulate Gate Bipolar Transistors," in *Proc. IEEE Congr. Evol. Comput. (CEC)*, Vancouver, BC, Canada, Jul. 2016, pp. 4705–4712.

[22] K. Stoyka, N. Femia, and G. Di Capua, "Power inductors behavioral modeling revisited," *IEEE Trans. Circuits Syst. I, Reg. Papers*, vol. 67, no. 12, pp. 5636–5649, Dec. 2020.

[23] K. Stoyka, R. A. P. Ohashi, and N. Femia, "Behavioral switching loss modeling of inverter modules," in *Proc. 15th Int. Conf. Synth., Modeling, Anal. Simulation Methods Appl. Circuit Design (SMACD)*, Prague, Czech Republic, Jul. 2018, pp. 1–20.

[24] J. R. Koza, "Genetic programming as a means for programming computers by natural selection," *Statist. Comput.*, vol. 4, no. 2, pp. 87–112, Jun. 1994.

[25] K. Deb, A. Pratap, S. Agarwal, and T. Meyarivan, "A fast and elitist multiobjective genetic algorithm: NSGA-II," *IEEE Trans. Evol. Comput.*, vol. 6, no. 2, pp. 182–197, Jan. 2002.

[26] C. A. Coello, G. B. Lamont, and D. A. Van Veldhuizen, *Evolutionary Algorithms for Solving Multi-Objective Problems*, 2nd ed. oston, MA, USA: Springer, 2007.

[27] D. P. Searson, "GPTIPS 2: An open-source software platform for symbolic data mining," in *Handbook of Genetic Programming Applications*, A. Gandomi, A. Alavi, and C. Ryan, Eds. New York, NY, USA: Springer, 2015.

[28] R. W. Kennard and L. A. Stone, "Computer aided design of experiments," *Technometrics*, vol. 11, no. 1, pp. 137–148, Feb. 1969.

[29] J. More, "The levenberg-marquardt algorithm: Implementation and theory," in *Numerical Analysis* (Lecture Notes in Mathematics), vol. 630, G. Watson, Ed. Berlin, Germany: Springer 1978, pp. 105–116.

[30] (Sep. 2019). *Data Sheets—Soft Ferrite Products and Accessories*. [Online]. Available: https://www.ferroxcube.com

[31] (Jan. 2021). *Productos: Hilo de Litz*. [Online]. Available: https://www.masfarne.com

ALBERTO DELGADO (Student Member, IEEE) received the B.Sc. degree in electrical engineering from the University of Málaga (UMA), Malaga, Spain, in 2016, and the M.Sc. degree in industrial electronics and the Ph.D. degree in electrical engineering from the Universidad Politécnica de Madrid (UPM), Madrid, Spain, in 2017 and 2021, respectively.

He became a Teaching Assistant with the UPM, in 2019. His research interests include modeling of dc–dc converters for inductive power transfer systems, magnetic components for different applications, such as RFID communications and wireless charging, and magnetic nanomaterials and micro-materials.

GIULIA DI CAPUA (Senior Member, IEEE) received the B.Sc. and M.Sc. degrees (Hons.) in electronic engineering and the Ph.D. degree in information engineering from the University of Salerno, Italy, in 2006, 2009, and 2013, respectively.

From 2013 to 2016 and from 2016 to 2020, she was a Post-Doctoral Researcher and a Research Assistant, respectively, both with the University of Salerno, Italy. Since 2021, she has been an Assistant Professor with the Department of Electrical and Informational Engineering, University of Cassino and Southern Lazio, Italy. Her research interests include power management, switching-mode power supplies optimization, magnetic components design, and wireless power transfer systems.

Dr. Di Capua is a member (and currently the Chair-Elect) of the Power and Energy Circuits and Systems (PECAS) Technical Committee of the IEEE Circuits and Systems Society (CASS). In 2017, she was the General Chair of the 14th International Conference on Synthesis, Modeling, Analysis and Simulation Methods and Applications to Circuit Design (SMACD 2017). She is the Track Chair on topics inherent to power systems and electronic circuits for flagship conferences of the IEEE CASS. She is an Associate Editor of the IEEE TRANSACTIONS ON CIRCUITS AND SYSTEMS—I: REGULAR PAPERS (TCAS-I).

KATERYNA STOYKA received the B.Sc. and M.Sc. degrees (Hons.) in electronic engineering and the Ph.D. degree in computer science and information engineering from the University of Salerno, Fisciano, Italy, in 2011, 2015, and 2019, respectively.

She has been a Research Fellow with the University of Salerno from 2019 to 2020. She is currently working as an R&D engineer in the Meditel s.r.l. company, Salerno, Italy. Her main research interests include analysis and design of switching mode power supplies, power magnetics, wireless power transfer systems, and numerical techniques for identification and optimization of behavioral models of power devices and systems.

LIXIN SHI (Student Member, IEEE) was born in Shijiazhuang, China. He received the master's degree in electrical engineering from Beijing Jiaotong University, Beijing, China, in 2016. He is currently pursuing the Ph.D. degree in power electronics with the Polytechnic University of Madrid, Madrid, Spain.

His research interests include wireless power transfer and resonant converters.

NICOLA FEMIA (Senior Member, IEEE) received the Laurea degree (Hons.) in industrial technologies engineering from the University of Salerno, Italy, in 1988.

He was an Assistant Professor, from 1990 to 1998, an Associate Professor, from 1998 to 2001, and since 2001, he has been a Full Professor of electrotechnics at the University of Salerno, where he teaches power electronics in the electronic engineering master's programs. He leads the Power Electronics and Renewable Sources Laboratory of the University of Salerno. In 2014, he has been a Visiting Professor with the Electrical Engineering Department, Stanford University, Stanford, CA, USA, where he taught power electronics control and energy aware design in the electrical engineering enhanced master's program. In the last two decades, he has directed and developed tens of research and education projects on power electronics topics, in collaboration with worldwide leader electronic companies. He held more than 50 invited lectures, courses, and seminars on power electronics design and education for universities and industries over Europe, USA, China, and India. He co-authored more than 200 scientific papers, one book, and seven patents. His research interests include circuit theory and applications, design and optimization of switching power supplies, magnetic power components modeling and optimization, power electronics and control techniques for photovoltaic systems, and wireless power transfer systems.

Prof. Femia was a member of the Administration Council of the University of Salerno, from 2002 to 2005. He was a member, and the Chairperson, from 2009 to 2010, of the Patents Council of the University of Salerno. He has been an Associate Editor of the IEEE TRANSACTIONS ON POWER ELECTRONICS, from 1995 to 2003.

ANTONIO MAFFUCCI (Senior Member, IEEE) received the Laurea degree *(summa cum laude)* in electronic engineering and the Ph.D. degree in electrical engineering from the University of Naples Federico II, Italy, in 1996 and 2000, respectively. In 1997, he was with the Nuclear Fusion Laboratory JET, Culham, U.K. From 1998 to 2002, he was with the Department of Electrical Engineering, University of Naples Federico II. He is currently a Full Professor of electrotechnics with the Department of Electrical and Information Engineering, University of Cassino and Southern Lazio, Cassino, Italy, and a Research Associate at the National Institute of Nuclear Physics, INFN-LNF, Frascati, Italy. He is the author of about 180 technical papers on international journals, conference proceedings, and essays on books. He also coauthored the books *Transmission Lines and Lumped Circuits* (Academic Press, 2001), *Fundamentals of Applied Nanoelectromagnetics* (Springer, 2016 and 2019), *Carbon Nanotube for Interconnects* (Springer, 2016), and *Carbon-Based Nano-Electromagnetics* (Elsevier, 2019). He is the Co-ordinator of the EU H2020-MSCA-RISE Project "Terasse" (2019–2023). His research interests include computational electromagnetics, electromagnetic compatibility, distributed circuit and systems, nanoelectronics, and quantum circuits. He is a member of the IEEE Nano-Packaging Council and of the Editorial Boards of Applied Sciences and of the *Journal of Nanoscience and Nanotechnology Applications*. He was a recipient of the Best Presentation Award at ENDE 2019, the Nanoscale Horizon Poster Prize at IEEE Nano 2015, the Best Paper Award at the IEEE Workshop SPI 2009, and the Outstanding Paper Award from Literati Network Awards for Excellence 2008. He served as the General Chairman for the conferences IEEE SPI 2011 and 2012, FANEM 2015 and 2018. He is an Associate Editor of the IEEE TRANSACTIONS ON COMPONENTS, PACKAGING, AND MANUFACTURING TECHNOLOGY.

SALVATORE VENTRE (Senior Member, IEEE) received the Laurea degree *(summa cum laude)* in electronic engineering from the University of Naples Federico II, Naples, Italy, in 1990.

Since 1993, he has been with the Department of Electrical and Informational Engineering, University of Cassino and Southern Lazio, Cassino, Italy, where he is currently an Associate Professor of electrotechnics. He has authored or coauthored more than 150 technical papers in international journals and conference proceedings. His current research interests include computational electromagnetic with application in several fields, such as electromagnetic nondestructive evaluation, electromagnetic compatibility, analysis of the time evolution of MHD equilibria, and for the identification of the plasma boundary in tokamaks.

PEDRO ALOU (Member, IEEE) was born in Madrid, Spain, in 1970. He received the M.S. and Ph.D. degrees in electrical engineering from the Polytechnic University of Madrid (UPM), Madrid, Spain, in 1995 and 2004, respectively.

He is currently a Full Professor with UPM. Since 1995, he has been involved in power electronics, participating in more than 70 research and development projects with the industry. He has authored or coauthored more than 45 journal articles, 140 conference papers, and holds six patents. His research interests include power converters, advanced topologies for efficient energy conversion, modeling of converters and magnetic components, advanced control techniques for high dynamic response, energy management, and new semiconductor technologies for power electronics. His research activity is distributed among industrial, aerospace, and military projects.

JESÚS ÁNGEL OLIVER (Member, IEEE) received the master's and Ph.D. degrees in electrical engineering from the Universidad Politécnica de Madrid (UPM), Madrid, Spain, in 1996 and 2007, respectively.

He became an Assistant Professor, in 2001, and an Associate Professor at UPM, in 2007. He has led numerous research projects with private and public funding, and he has participated in more than 50 direct research and development projects with companies in Europe, USA, Australia, and China. He has been the author or coauthor in more than 150 scientific papers on journals and conferences and he holds five patents. His research interests include modeling (dc–dc converters, magnetic components, piezoelectric transformers, fuel-cells, and dc distributed power electronic systems), fast control techniques for dc–dc converters for VRM applications and RF amplifiers, three-phase rectifiers for aircraft applications, wireless power transfer, and power systems on chip.

JOSÉ ANTONIO COBOS (Fellow, IEEE) received the master's and Ph.D. degrees in electrical engineering from the Polytechnic University of Madrid (UPM), Madrid, Spain, in 1989 and 1994, respectively.

In 2006, he became the Founder Director of the Centro de Electrónica Industrial at UPM (CEI-UPM), a university research center leading a strong industrial program in power electronics and digital systems. In 2016, he became the Founder President of its Industrial Council, to coordinate education and research with industry. He is currently a Full Professor with the UPM. His contributions are focused on power supply systems for industrial, aerospace, telecom, automotive, renewable energy, and medical applications. He advised more than 50 graduate students, published more than 300 technical articles, and is a co-inventor of patents with eight companies. His current research interests include energy efficiency in digital systems, RF amplifiers, renewable energy, magnetic components, transcutaneous energy transfer, and biomedical applications.

Dr. Cobos was an Adcom Member of the Power Electronics Society (IEEE-PELS) and the Chair of its Technical Committee on dc power supply systems. He was the General Chair of Power Supplies on-Chip (PwrSoC) 2016, IEEE-PELS, and PSMA. He conducted professional seminars and tutorials in USA, U.K., Austria, Germany, Italy, Sweden, Switzerland, Syria, Mexico, and Macedonia. He is a Steering Committee Member and the General Chair of IEEE-APEC'2020, the Largest Power Electronics Conference and Exhibition in the USA, with 5 000+ attendees. During 2016–2017, he was an RCC Fellow at Harvard University and a Fulbrighter with the University of California at Berkeley, USA. He received some international recognitions as the Semikron Innovation Award, the Google Little Box Challenge award for Universities, and the Outstanding Young Power Electronics Engineer Award of IEEE-PELS. In 2019, he founded ''Differential Power S.L.'', a startup awarded second prize in ActúaUPM, to develop IP that enable next-level supply of A.I. chip. He was an Associate Editor of the IEEE Transactions on Power Electronics and the IEEE Power Electronics Society Letters.

• • •